Methods and Applications in Fluorescence

A first approach to the use of upconversion nanoparticles to measure fluorescent tracers in water: A proof of concept

To cite this article before publication: Juan M. Bujjamer *et al* 2021 *Methods Appl. Fluoresc.* in press https://doi.org/10.1088/2050-6120/ac2e99

IOP Publishing Journal Title
Journal **XX** (XXXX) XXXXXX https://doi.org/XXXX/XXXX

A first approach to the use of upconversion nanoparticles to measure fluorescent tracers in water: A proof of concept

Juan M. Bujjamer[1], Marcos Illescas[2], M. Claudia Marchi[2,3], Hernán E. Grecco*[1,3]and Beatriz C. Barja*[2,4]

[1] Departamento de Física, Facultad de Ciencias Exactas y Naturales (FCEN), Universidad de Buenos Aires (UBA), Ciudad Universitaria, Pabellón 1, C1428EHA Buenos Aires, Argentina.
[2] Departamento de Química Inorgánica, Analítica y Química Física, FCEN, UBA, Ciudad Universitaria, Pabellón 2, C1428EHA Buenos Aires, Argentina
[3] Instituto de Física de Buenos Aires-CONICET, Ciudad Universitaria, Pab. 1, C1428EHA Buenos Aires, Argentina.
[4] INQUIMAE-CONICET, Ciudad Universitaria, Pab. 2, C1428EHA Buenos Aires, Argentina.

E-mail addresses: barja@qi.fcen.uba.ar and hgrecco@df.uba.ar

Received xxxxxx
Accepted for publication xxxxxx
Published xxxxxx

Abstract

In this work we use lanthanide based $NaYF_4$:Er^{3+}, Yb^{3+} upconversion nanoparticles (UCNP) to detect ppb-level sensitibity of a xanthene dye, Rhodamine B (RB) dye, under NIR excitation. A static energy transfer was observed between the luminescent UCNP energy donors and RB acceptor in aqueous solution for three different sizes of UCNP. No specific covalent functionalization of the UCNPs was performed providing a direct method of detection, particularly promising in natural systems where the interfering fluorescence background is a detrimental limitation to the performance of the detection method. This procedure is a first approach to be applied in estuarine and coastal zone where the high content of suspended particulate matter prevents the detection of tracers.

Keywords: upconversion, tracers, sensing

1. Introduction

Fluorescent tracers are dyes widely used in hydrology for dispersion and transport studies in surface water and groundwater systems. The addition of a tracer to a water body enables the tracking of water pathways and flow rates through the system to determine, for example, residence times or pollutant concentrations [1][2][3]. Not less important is the use of these tracers to validate or verify the different transport models proposed to study the evolution of the system [4].

Some of the most used fluorescent tracers are derived from the xanthene core such as Rhodamine or Fluorescein derivatives. Since Rhodamine B (RB) is soluble in water, highly fluorescent dye with low toxicity (lethal dose LDLo = 500 mg/kg, oral-rat) [5] this substance is currently used to investigate the transport and the turbulent diffusion of conservative constituents in water bodies. Excellent reviews and summaries are available on the use and characteristics of fluorescent dye tracers [6] [7].

The key problem when measuring the concentrations of a tracer by fluorescent techniques in natural systems is the limitation determined by the background of the sample: the

natural fluorescence and the suspended sediment. The suspended material which varies strongly with topography and tidal current interferes the studies because the light scattered from the exciting beam may lead to a background signal comparable to the signal expected from the dye itself at low levels [8]. The background fluorescence is derived from naturally-occurring organic compounds, organisms [9] such as bacteria, algae and higher plants, as well as a wide range of manmade chemicals, including compounds from the petroleum, paper and agrochemical industries. Many of these fluorescent substances might share excitation or emission spectra with the tracers, and thereby severely interfere in the determination of the dye. The naturally occurring background fluorescence of surface waters can be relatively high particularly for fresh water and estuarine water. In sea-water, detection limits of the order of 5×10^{-11} g/ml are achieved. In estuaries, the high content of suspended particulate matter deteriorates to levels as high as 10^{-8} g/ml. In fact RB could not be detected in the estuarine and coastal zone because its signal was lost in the natural background [10]. In view of these facts, new detection methodologies are required to overcome the detrimental effects caused by the natural fluorescence background of the systems under study.

If it were possible to develop a sensor in which the source of light was transparent to the background fluorescent components but detected by a target tracer, it would benefit markedly the analytical performance of the method, particularly the sensitivity and detection limits. With this idea in mind, we propose to take advantage from the upconversion emission properties of the lanthanides ions to introduce a new conceptual methodology to monitor a fluorescent tracer.

The process of upconversion (UC) is one of the most fascinating features that lanthanide ions can offer from an energetic point of view. Contrary to conventional high energy excitation, the mechanism of photon upconversion (UC) converts a long-wavelength infrared excitation radiation into a shorter wavelength (visible) output radiation [11]. This unique type of luminescence at a nanoscale level results extremely attractive and has been intensively pursued, not only for their scientific interest, but also for their many technological and biological applications [12][13]. The synergy between UC and optical sensing techniques has promoted the development of innovative monitoring strategies and recent reviews evidence the state of art of this new approach [14] [15] [16][17].

Given their electronic properties, the lanthanide ions can absorb more than one photon of the same near infrared energy in a sequential way [18]. Such two, three and even four-fold sequential absorption enables the emission of much higher energy radiation in the visible and even ultraviolet range. This anti Stokes process can be achieved using inexpensive, CW laser diodes or LEDs in the NIR with low power densities (1 W/cm^2). The most studied UC material is based on a hexagonal β-$NaYF_4$ matrix doped with Yb^{3+} and Er^{3+} ions where the excitation source can be chosen with low excitation intensity (1 - 10^3 W/cm^2), such as cheap and readily available continuous wave diode lasers [19]. These upconversion nanoparticles (UCNP) were successfully applied during the last decade in fields as diverse as chemical sensing 20], security [21], photonics [22] and bioimaging where a deeper penetration is needed with no degradation or bleaching [23].

In the present study, we synthesized three different UCNP based on a β-$NaYF_4$ matrix codoped with Yb^{3+} (20%) and Er^{3+} (2%) with different diameter/length ratios and a fourth one with a passivated shell. The emission spectra of these UCNP fully overlap the absorption spectra of the model xanthenic tracer RB enabling their use as energy donors in an energy transfer (ET) process. We studied this energy transfer processes by steady-state and time-resolved luminescence spectroscopy under 976 nm NIR excitation from a low power diode laser. Detection limits in the order of 30 ppb were achieved from deactivation studies, which are low enough to be used in estuarine and coastal zones where the signal is generally lost.

2. Experimental

All lanthanide chlorides, oxides, oleic acid (90%), 1-octadecene (90%), oleylamine (90%), ammonium fluoride (99.99%), trifluoroacetic acid, sodium hydroxide, ammonium hydroxide, dichloromethane (DCM), ethyl ether (anhydrous), dimethylformamide (DMF), hexane and polyvinylpyrrolidone 15 kg mol^{-1} (PVP15) were purchased from Sigma-Aldrich. All chemicals were used as received without further purification.

2.1 Synthesis. The β-$NaYF_4$:Yb^{3+}(20%), Er^{3+}(2%) upconversion nanoparticles were synthetized by a thermal decomposition method starting from the lanthanides precursors chlorides (Cl-C [24]) or trifluoroacetates, (TFA1 [25] and TFA2[26]) changing the solvent, surfactant, time and temperature of heating. In a typical synthesis, 0.78 mmol of the Yttrium precursor, 0.20 mmol of the Ytterbium precursor and 0.02 mmol of the Erbium precursor were added to a 100 mL three-necked flask containing the surfactant (6 mL) and the solvent (15 mL). The solution was stirred and heated to 150°C under vacuum for 30 min to get homogeneous solution and then cooled down to room temperature. A solution of NH_4F (4 mmol) and NaOH (2.5 mmol) dissolved in methanol (10 mL) was added and then heated slowly to 70°C until all the methanol evaporated. Subsequently, the solution was heated to 300-330°C for 60 min-120 min (see Table 1) under argon atmosphere. In the case of the TFA precursors, 2 mmol of $NaCF_3COO$ were also added to the flask with the rest of the TFA precursors and the synthesis was performed in one step, with no NH_4F addition. The UCNP were precipitated by adding ethanol, centrifuged and washed with hexane and ethanol three times.

Cl-CS. Half of the Cl-C nanoparticles were coated with a shell of $NaYF_4$ free from dopants: 2 ml of a suspension of Cl-C in hexane were added to a mixture of 0.78 mmol of $YCl_3.H_2O$ dispersed in oleic acid (OA, 6ml) and octadecene (OD, 15 ml). After stirring, 5 ml of methanol containing 4 mmol of NH_4F and 2.5 mmol NaOH were added and the mixture was heated at 70°C to eliminate the alcohol. The system was purged alternating vacuum and argon cycles and then heated under stirring at 300°C during 45 min. Once the system was at room temperature, the *core shell* Cl-CS particles were precipitated with ethanol, washed and kept in hexane. A heating ramp of 70°C/min was applied from a PID-thermocouple controller to keep reproducible experimental conditions.

2.2 Morphological and structural characterization. A X-ray powder diffractometer (Panalytical Empyrean) with Cu Kα radiation (λ = 1.5406 Å) at 40 kV and 45 mA was used to collect the phase structure of as-synthesized samples at room temperature. Diffractograms were recorded in the 10-90º 2θ range with a scan step of 0.026° and 50 seconds/step. All the diffraction peaks can be indexed to those of pure phase-hexagonal β-$NaYF_4$:Yb^{3+}(20%), Er^{3+}(2%) structure (space group: $P6_3/m$) in good agreement with the Joint Committee on Powder Diffraction Standards (JCPDS No. 16-0334). No other impurity peaks were detected, pointing out the single-phased nature of the nanocrystals. The average crystallite size are listed in the Table 1. The XRD patterns of the samples are shown in Figure S1.

The size and morphology of the samples were measured with a field emission scanning electron microscope (FESEM, Zeiss Supra 40) and are shown in Figure 1. The UCNP were dispersed in ethanol and dropped on the surface of a silicon wafer for FESEM characterization. All synthesized β-$NaYF_4$:Yb^{3+}, Er^{3+} nanoparticles are hexagonal shaped prisms with different diameter/length aspect ratios.

Direct evidence of the formation of core/shell structure is given by the increase in the size of the initial core UCNP together with an enhancement of the UC luminescence and longer decay times. In our case the SEM micrographs show an increase of 17% and 36% in the diameter and in the length of the Cl-CS UCNP respectively when compared with the core Cl-C sample. The epitaxial growth of the Cl-CS nanoparticles determined a more clearly defined hexagon shape when compared with the core only sample rendering a brighter emission.

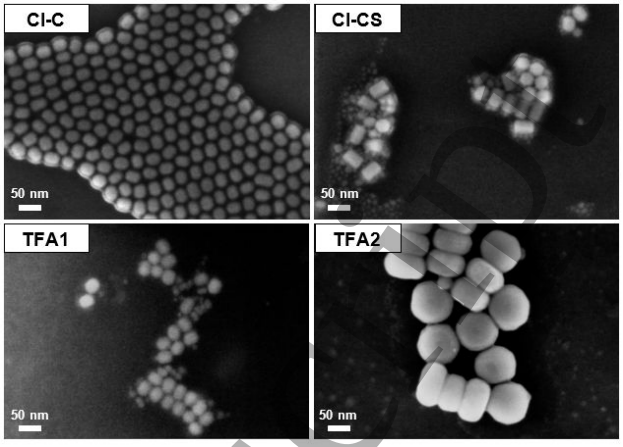

Figure 1: SEM images of the UCNP samples.

2.3 Ligand exchange treatment. The procedure was taken from reference [28] with minor differences. In a 100 ml round bottom flask containing 5 ml of a mixture of a 1:1 DMF: DCM, were added 0.85 mg of PVP15 under stirring. After dissolution of the solid, 0.2 ml of a 4% m/V dispersion of the synthetized β-$NaYF_4$:Yb^{3+}/Er^{3+} in hexane were added to the mixture and refluxed at 100°C for 6 h. Once the mixture is at room temperature, the reaction mixture was added dropwise into ethyl ether (60 ml) to precipitate the PVP-stabilized nanoparticles. The white precipitate was centrifuged at 4000 rpm during 5 min and the precipitate was transferred to 4 ml of Milli-Q water to yield a transparent and stable aqueous dispersion of the PVP-stabilized $NaYF_4$ nanoparticles.

2.4 Spectroscopic Measurements:

Stationary emission measurements: The emission spectra were acquired with a spectrofluorimeter (Horiba PTI QuantaMaster) equipped with a photomultiplier tube (PMT) and a 976 nm coupled laser diode fiber (300 mW, Thorlabs BL976-SAG300).

The emission wavelength was swept from 350 to 700 nm with a a step size of 1 nm at 0.5 s/nm. The samples were measured at room temperature in 1.00x1.00 cm quartz cells.

Time-dependent emission measurements. The lifetime measurements were obtained from a photon counting system

Sample Code	Solvent	Surfactant	Time (min) - Temp (°C)	Diameter (nm)	Length (nm)	Crystallite Size (nm)
Cl-C	OD	OA	120 - 300	29 ± 2	38 ± 2	29.7
Cl-CS	OD	OA	45 - 300	34± 3	52 ± 5	31.2
TFA1*	--	OAm	60 - 330	31 ± 1	37 ± 2	32.3
TFA2*	OD	OA	90 - 340	102 ± 3	60 ± 4	36.9

Table 1: Sample code, synthesis conditions (solvent, surfactant, time and temperature), average diameter and length of UCNP, and their crystallite size. (*) The $Yb(TFA)_3.3H_2O$ was synthetized from the oxides [27]. OAm refers to oleylamine.

coupled to the previously described Horiba PTI QuantaMaster spectrofluorimeter. The counting mechanism was implemented with a FPGA microcomputer as an analog acquisition system (Red Pitaya 125-14) and the samples were excited with a square laser 976 nm. We used less than 5% of the maximum bandwidth of the detector to avoid pulse pile-up effect..

3. Results and Discussion

3.1 Optical characterization:

Figure 2 shows the UC emission spectra of the UCNP in hexane upon excitation at 976 nm. The spectra show the typical narrow bands of the emission of the Er^{3+} ions in the green (500-570 nm), and red (630-690 nm) regions as a result of the $^4S_{3/2}$,$^2H_{11/2}\rightarrow{}^4I_{15/2}$ and the $^4F_{9/2}\rightarrow{}^4I_{15/2}$ intra f-f transitions, respectively. The weaker bands in the blue and NUV arise from the $^2H_{9/2}\rightarrow{}^4I_{15/2}$ (410 nm) or $^4G_{11/2}\rightarrow{}^4I_{15/2}$ (383 nm) transitions.

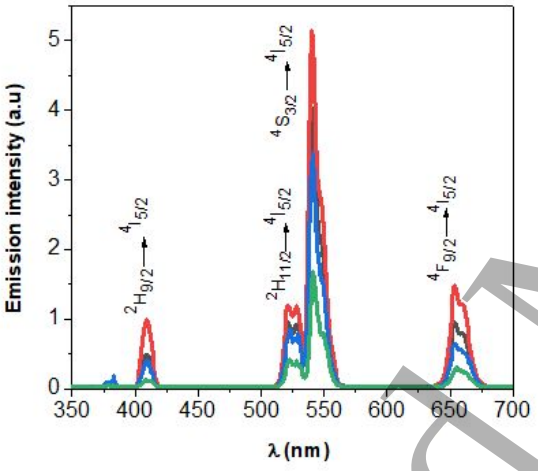

Figure 2: UC emission spectra of the four synthesized UCNP in hexane upon excitation at 976 nm. Red (Cl-CS; 0.13 mM), Black (Cl-C; 0.33 mM), Blue (TFA1; 5 mM) and green (TFA2, 3 mM).

The mechanism for the red and green UC emission is depicted in Figure 3 [29][30]. Upon excitation, a 976 nm photon promotes the sensitizer Yb^{3+} ion from the $^2F_{7/2}$ ground state to the $^2F_{5/2}$ excited state. An energy transfer-upconversion process (ETU) takes place and the activator ion Er^{3+} in the $^4I_{15/2}$ ground state is promoted to the $^4I_{11/2}$ excited state while the Yb^{3+} ion returns to its $^2F_{7/2}$ ground state simultaneously. This ETU process can be repeated and after the absorption of a second 976 nm photon, the Er^{3+} ions can be promoted from the $^4I_{11/2}$ to an even higher $^4F_{7/2}$ excited state meanwhile the sensitizer returns to its ground state. Subsequently, after one or more non-radiative decay steps Er^{3+} can emit green photons from the $^2H_{11/2}$ or $^4S_{3/2}$ excited states or alternatively red photons from the next lower lying $^4F_{9/2}$ state. Emission from higher levels $^2H_{9/2}\rightarrow{}^4I_{15/2}$ or $^4G_{11/2}\rightarrow{}^4I_{15/2}$ arise from the absorption of at least three 976 nm photons and are not shown.

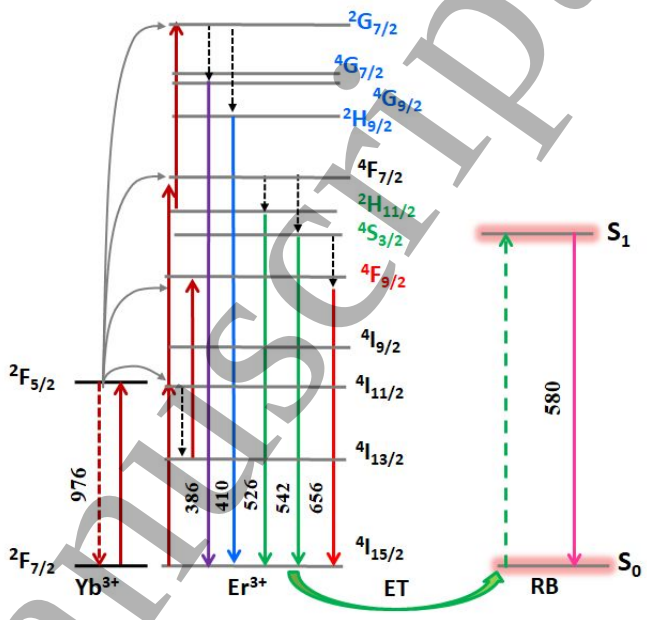

Figure 3: Energy levels and simplified mechanism of upconversion processes in $NaYF_4$: Yb^{3+}, Er^{3+} at an excitation wavelength of 976 nm. The ground and excited states of RB are included together with the energy transfer process (ET).

The spectra show that the UCNP coated with a $NaYF_4$ shell (Cl-CS) is the most luminescent sample, even when its concentration (0.13 mM) is 3, 38 and 23 times lower than Cl-C, TFA1 and TFA2, respectively. This inert shell isolates the dopant ions of the core preventing non radiative energy losses from the surface to the solvent or other eventual quenchers. In particular, when the matrix of the core and the shell are the same ($NaYF_4$) no lattice mismatch is present and surface-related deactivation mechanisms [31] are largely suppressed yielding more efficient radiative processes [32].

It is important to note that in Figure 2 the most intense emission band are located in the green region (500 nm – 575 nm), with green/red area ratio of 3.9 ± 0.5. A key point to fulfill the requirements of an energy transfer process relies on the degree of overlap between the emission spectrum of the donor (D) and the absorption spectrum of the acceptor (A). Figure 4, shows the huge overlap between the green emission of the UCNP donors and the absorption spectra of the RB acceptor, suggesting that a monitoring system to detect RB can be envisaged using UCNPs as donor entities. This overlap is represented in the scheme in Figure 3 by the inclusion of the ground state and excited orbitals of the RB in the energy levels. The red emission of the UCNP shows no band superposition with the absorption of the RB not interfering the analysis of the energy transfer process.

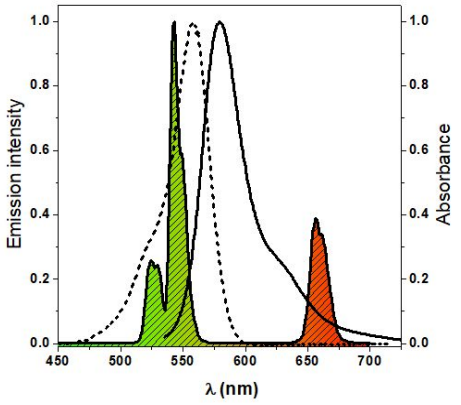

Figure 4: Normalized spectral overlap between the green emission spectrum of the UCNP (shaded green area) and the absorption spectrum of the RB (dashed line). RB emission is shown in solid black line.

Emission spectra in water before and after the oleate-PVP exchange: All the UCNPs were synthesized via a thermal route at elevated temperatures in the presence of surfactants and solvents of high boiling points. The surfactants contain a polar carboxylate (Oleic acid, OA) or an amine (Oleylamine, OAm) capping group capable to coordinate the lanthanide ions at the surface of the UCNP while the long hydrocarbon chain extends in the nonpolar solvent preventing nanoparticle aggregation, being the hydrophobic layer of oleic acid of about *~1.1 nm thickness*. [33] This route of synthesis guarantees precise control over the phase, shape, size, dispersion and stoichiometric composition of the UCNP, as observed by SEM and XRD characterization methods. As a consequence of this treatment, the UCNP are hydrophobic and dispersible in nonpolar organic solvents. To make the UCNP soluble in water it is necessary to modify their surface. There are several strategies to achieve this goal with different grades of complexity [34]. In this work we opted for a simple ligand exchange method under the premise that the chosen procedure would not be expensive, straightforward, and environmentally friendly. PVP is a non-toxic, cheap, non-ionic polymer that has been widely used in the synthesis of nanoparticles [35]. PVP contains a highly polar pyrrolidone moiety as well as hydrophobic alkyl groups in the ring and along its backbone enabling its solubility in water and many non-aqueous liquids, stabilizing the UCNP dispersions [36]. In aqueous solution, PVP acts as a Lewis base and adsorbs on an oxide surface via the carbonyl bond [37] as well as on Ag nanoparticles.[38] Most interesting, it was shown that the carbonyl moiety of the pyrrolidone group can coordinate the lanthanide ions and complexes [39] [40] helping to prevent non radiative processes. Figure 5 shows the emission spectra of dispersions of sample Cl-C in water before and after the PVP exchange in the same experimental conditions. The spectrum of Cl-C without PVP is very noisy and difficult to reproduce because the dispersions are very unstable and the particles tend to agglomerate easily, even under stirring and sonication. After the PVP treatment, the particles are easily dispersed in water, the dispersions are stable and transparent, and their emission spectra can be obtained with an excellent reproducibility even after several weeks.

The oleate-stabilized UCNP with no PVP treatment are less bright in aqueous dispersions that in hexane as a consequence of the non-radiative deactivation of the excited Er^{3+} ions caused by the high phonon energy of O–H oscillators of the water molecules. The quenching process in lanthanide excited states by O–H vibrations has been widely reported [41][42.] Fortunately, in the presence of PVP polymer, the water molecules do not affect the green to red intensity ratios of the UCNP evidencing certain degree of shielding for the non-deactivation of the 534 nm band. This protecting effect of PVP from the surrounding water molecules was also observed in silver nanoparticles.[43]

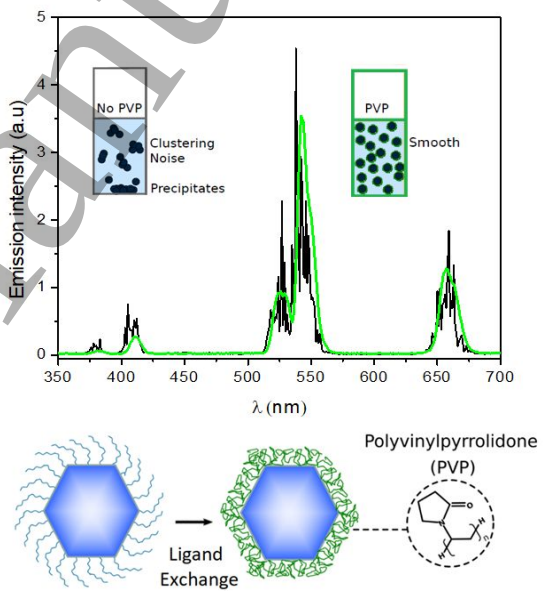

Figure 5: UC emission spectra of Cl-C in water with PVP (green line) and without PVP (black line) (left) under λ_{exc} = 976 nm.

3.2 Luminescence measurements: Quenching processes

Figure 6 depicts the emission spectra of the four samples. This figure shows that the green upconversion emission at 534 nm decreases in all samples upon addition of μmoles of RB, with the concomitant appearance of the emission band of the RB centered at 580 nm. Given that the incident light at 976 nm can be absorbed only by the ions in the UCNP this is a conclusive demonstration that an energy transfer process from the UCNP to the acceptor dye RB is taking place.

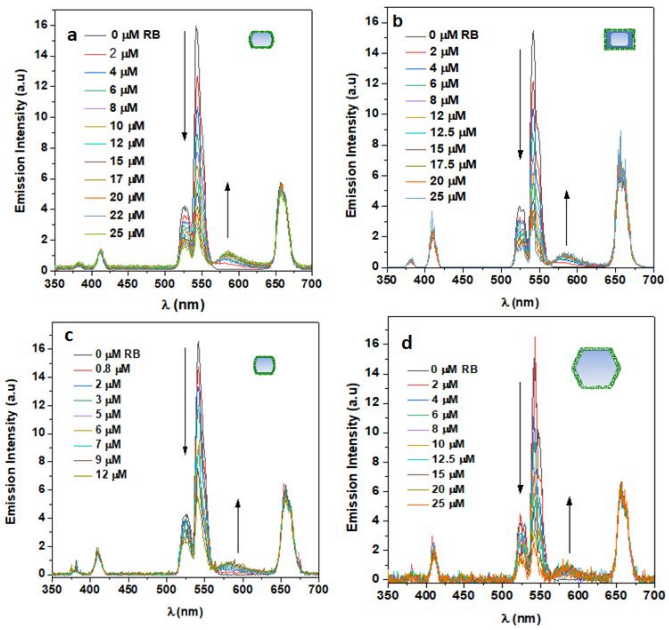

Figure 6: Emission spectra of the PVP modified UCNP Cl-C (a), Cl-CS (b), TFA1 (c) and TFA2 (d) excited at 976 nm in aqueous solution under incremental additions of RB. The arrows point out the decrease of the intensity of the green bands of the UCNPs (525-560 nm) together with the enhancement of the RB emission at 580 nm.

The excited state lifetimes of the PVP coated UCNP measured at 512 nm under 976 nm excitation without (τ_0) and with (τ) the addition of RB are shown in Table 2. These results indicate that the values of the excited lifetimes τ do not change significantly from τ_0 (140 ± 1 μs) with the addition of RB in the 0 – 10 μM of RB. The uniformity in the values of the lifetimes indicates that the deactivation process of the emission of the UCNP by RB are static in nature and the quenching should be explained in terms of a static mechanism.

RB (μM)	Lifetime τ (μs) at 542 nm	$\%E = 1 - {}^{\tau_0}/_{\tau}$	$\%E = \left(1 - {}^{I}/_{I_0}\right).100$
0	140 ± 1	-	-
1.2	130 ± 1	7	1-(2.1/2.6)= 19
2.4	140 ± 1	-	-
4.7	130 ± 1	7	1-(1.55/2.6= 41
9.4	130 ± 1	7	1-(1.25/2.6)= 52

***Table 2**: Excited states lifetimes of the PVP coated UCNP in HEPES monitored at 542 nm under 976 nm excitation without (τ_0) and with (τ) the addition of RB. ET efficiency are shown for Cl-CS UCNP*

The possibility of a dynamic quenching is evidenced by the change in the excited state lifetime at 542 nm of the UCNP donors with (τ_0 = 130 μs) and without (τ_0 = 140 μs) the acceptor RB. However, this 7% change in the energy transfer process cannot explain the observed 41% and 52% decrease calculated from the intensity values.

As expected, the excited state lifetime at 658 nm did not change upon RB additions ($\tau_0 = \tau$ = 350 μs) in accordance to the absence of spectral overlap view that no spectral overlap is present in this band.

.

3.3 Quenching Experiments: To evaluate the performance of the UCNP-RB system, we carried out the quenching experiments of the PVP coated UCNP dispersed in HEPES by addition of micromoles of RB. For direct comparison, the experimental conditions were kept constant for all of the titrations: 0.67 mg of PVP coated UCNP dispersed in 2.5 mL of HEPES (pH=7) were placed in a 1 cm quartz cuvette under stirring and titrated with different microliters of a 2.0×10^{-4} M aqueous RB using a 0-5 μL Hamilton microsyringe. The excitation wavelength was kept at 976 nm at constant low powers and the emission spectra were scanned in the 350 to 700 nm range. The step size was 1 nm at a scan velocity of 0.2 to 0.5 s/nm. According to the Stern Volmer equation (Eq.1) the I_o/I values were plotted against the RB concentration and the results are shown in Figure 7.

$$\frac{I_0}{I} = 1 + K_{SV}[RB] \qquad Eq.1$$

I_o and I represent the emission intensity of the UCNP at 534 nm without and with the addition of RB, respectively. The parameters obtained from the linear fit together with the detection limits (LOD) of RB for each sample are summarized in Table 3.

For static quenching, the dependence of the emission intensity upon quencher concentration is derived by considering an association or complexation process governed by a constant for a non-luminescent entity between the emitting species and the quencher RB [44] and hence $\tau_0 = \tau$ at any concentration of quencher because the excited state is not being depopulated. It is assumed an encounter between

the D and the A to form a dark complex in the ground state

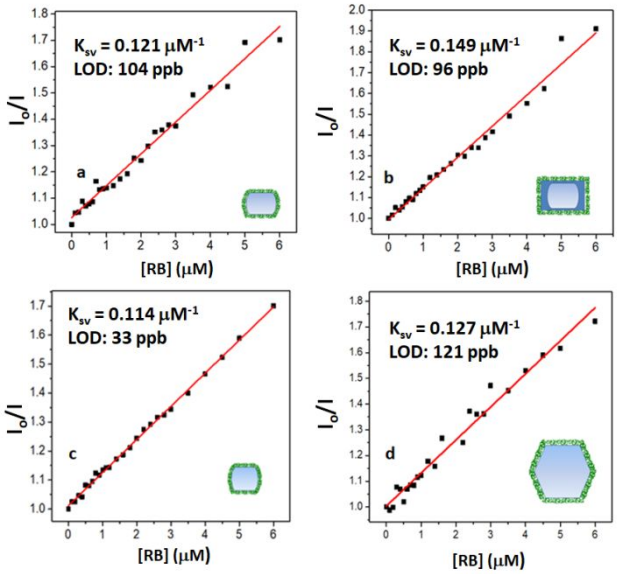

Figure 7: Stern Volmer plots obtained from the spectra of Figure 6. The UCNPs Cl-C (a), Cl-CS (b), TFA1 (c) and TFA2 (d) were drawn to scale. LOD= $3s_a/b$, where s_a is the error of the fit and b is the slope or gradient of the fit.

The invariance of the lifetime would typically be modeled as a static Stern-Volmer mechanism. Nevertheless, our systems do show a significant amount of energy transfer that we should take into account in our model.

In a static energy transfer process, the energy is transferred to the acceptor after the radiative relaxation of the donor, and the acceptor absorbs the emitted photon. This radiative energy transfer is an emission-reabsorption process where the temporal behavior of the donor emission is not affected keeping the lifetime at a constant value with or without acceptor. The result is a decrease of the donor emission intensity in the region of the spectral overlap. The efficiency of this process is determined by the quantum yield of the donor emission and the absorption acceptor at the donor emission wavelength. Static ET drops off with the inverse square law in relation with the cross section of the acceptor and is much less sensitive to the donor−acceptor distance than a dynamic ET.

On the basis of these facts, we attribute the quenching mechanism of the PVP modified UCNP to an emission-reabsorption effect in which the light emitted from the nanoparticle is absorbed by the dye present in the solution. As the RB concentration values range are in the micromolar range, an inner filter effect for RB itself was discarded [45]. The K_S obtained from the experiments are in the order of 0.1-0.15 μM^{-1} indicating that the sensitivity of the method, given by their slopes, is practically independent on the size of the UCNP. This is a quite interesting result and could be interpreted in terms of a similar and uniform distribution shell of the PVP around the UCNP. The accessibility of the RB to the UCNPs seems to be governed by the PVP polymer. Interestingly, it was reported [46] that the photophysical and photochemical properties of the xanthene dye Rose Bengal were modified in presence of a polymer such as PVP in aqueous solutions. A most likely hydrophobic dye-polymer interaction seems to minimize the less favorable dye-solvent interactions reducing the non-radiative deactivation pathways. The lower polarity environment experienced by the dye decreases the molecular diffusion processes through the polymer, what could explain the entrapment of the dye by the polymer shell that surrounds the UCNP.

Table 3 summarizes the fitting data and UCNP sizes.

Sample	K_{SV} (μM^{-1})	R^2	Size (nm)	LOD (ppb)
Cl-C	0.114 ± 0.001	0.9977	38 × 29	33.2 ± 0.5
Cl-CS	0.149 ± 0.004	0.9727	52 × 34	96 ± 4
TFA1	0.121 ± 0.003	0.9794	37 × 31	104 ± 4
TFA2	0.127 ± 0.004	0.9763	60 × 102	121 ± 5

Table 3: Linear fit parameters and detection limits. LOD (ppb): $3s_a$/slope.

Similar Stern Vomer plots for PVP-free UCNP showed no reproducible results due to particle aggregation or precipitation giving in return highly noisy spectra from which no reliable information could be extracted. These results are not shown.

From the plots in Figure 7, a linear relationship was obtained in the range of 0 - 6 μM RB where the green emission of the UCNP decreases with the simultaneous enhancement of the RB band at 580 nm. For concentrations higher than 10 μM of RB, this energy transfer mechanism was no longer observed since the fluorescence of the RB remained constant even though the UC emission of the UCNP at 534 nm kept on decreasing. This trend is represented by the plateau observed in Figure 8 by the integrated areas of the emission of the RB at 580 nm together with the emission of the UCNP-PVP at 534 nm. These results indicate that at these saturation levels, the radiative emission by the UCNP is no longer transferred to the dye ending up as heat in the solution. The fitting parameters of the plots in Figure 9 are shown in Table S2. The theoretical saturation values were calculated from the SEM sizes, reported bibliographic values [33] and experimental data (Supplementary Information, Table S1, row 7) and are in agreement with the range of the experimental values obtained from the saturation values at large RB concentrations (see Figure S2).

Static energy transfer mechanisms were observed in many systems, particularly when polymers or large organic

molecules and biomolecules are in the presence of UCNP [47][48][49][50]. The interplay between static and dynamic energy transfer was studied in detail for $NaYF_4$: Er^{3+}/Tb^{3+} nanoparticles with Rose Bengal as photosensitizer and it was observed that the static energy transfer increased when the shell of the UCNP gets thicker [51][52]. ($NaYF_4$:Yb^{3+}, Er^{3+}) UCNP were reported to detect 0.01 μM levels of Cr(VI) based on static energy transfer effect [53].

Sphere of effective quenching: The term static quenching implies either the existence of a sphere of effective quenching or the formation of a ground-state non-fluorescent complex [54]**.** We opted to apply this sphere of action model to seek for further information. When the excited donor and the quencher cannot change their positions relative to one another during the excited-state lifetime of the donor because it is somehow impeded by the viscosity of the media or the matrix, a model called the sphere of effective quenching or sphere of action can be applied. The quenching of the fluorophore is assumed to be complete if the quencher is located inside this sphere of volume V_q surrounding the fluorophore. Outside this sphere, no quenching occurs. Therefore, the fluorescence intensity is decreased by addition quencher Q, but the fluorescence decay is unaffected and $\tau_0/\tau = 1$. The probability that n quenchers reside within this volume is assumed to obey a Poisson distribution Eq (2):

$$P_n = \frac{< n >^n}{n!} = \exp(-< n >) \quad \text{Eq (2)}$$

where <n> is the mean number of quenchers in the volume V_q : <n> = $V_q N_a[Q]$ (V_q is expressed in L, [Q] in mol L^{-1}, N_a is Avogadro's number). The probability to find no quencher in this volume P_o (n=0) is:

$$P_0 = \exp(-\langle n \rangle) = \exp(-V_Q . N_a[Q]) \quad \text{Eq (3)}$$

Being the emission intensity proportional to P_o:

$$\frac{I_0}{I} = \exp(V_q N_a[Q]) \quad \text{Eq (4)}$$

At low concentrations, exp (V_qNa[Q]) ≅ 1 + $V_q N_a$[Q] and the concentration dependence with I_o/I is almost linear. A plot of $\ln(I_o/I)$ versus [Q]=[RB] yields V_q. Figure 8 shows the fit obtained from a graph of $\ln(I_0/I)$ against [RB] together with the values obtained for the radii of the sphere of action Vq.

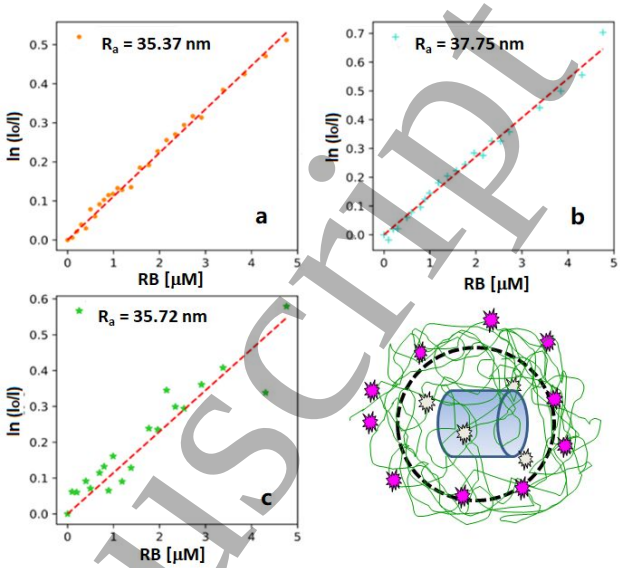

Figure 8: Sphere of effective quenching mdels for PVP coated Cl-C (a), Cl-CS, (b) and TFA1 (c) UCNP. In all cases, an average sphere of action radius about 35 nm was found (dashed circle). PVP is represented by the green strings, and RB as stars. In this model, the UCNP can transfer its energy radiatively to the RB molecules inside the effective sphere but not outside.

We found a similar sphere of action radius of 35 ± 3 nm for the PVP coated UCNP. Considering that the radii obtained by SEM are Cl-C (14.5 nm), Cl- CS (17 nm) and TFA1 (15.5 nm) there would be an extra average radial distance of about 20 nm where the RB can locate. In the case of TFA2, a good fitting was not possible, maybe due to its planar platelet shape, far from spherical as specified in Possion distribution. Compared with SEM, a larger different diameter can be attributed to the swelling effect of the wrapped polymer coating. As reported by Muhr et al [50], dynamic energy transfer efficiencies up to 60%, were achieved in DMF for smaller UCNP@Rose Bengal of 21 nm diameters sizes. Accordingly, a reduction in the size of the UCNPs could potentially enhance the performance of the sensors presented here, changing the organic solvent to water.

4. Conclusions

In this work we propose the use of UCNP as energy donors' entities to detect traces of an acceptor xanthene-type RB in aqueous solution using 976 nm light as the excitation source. In this strategy, where no specific covalent surface functionalization of the UCNP was necessary, the detection

limits attained (LOD= 30 ppb) are in the range of those reported in estuarine or coastal zones (10^{-8} g/ml) using much more expensive equipment. In fact, RB could not even be detected in the estuarine and coastal zone because its signal was lost in the natural background. The quenching experiments showed that a static radiative energy transfer process was taking place in the system up to a given saturation RB concentration from which the emission of the UCNP was no longer absorbed by the RB but dissipated as heat. To our knowledge this is the lowest detected value of RB using UCNPs as energy transfer entities [55].

Acknowledgements

We acknowledge UBACyT 2018-2020 (2002017010755BA) project, ANPCyT (PICT-2013-1301) and FAN (PreSemillas) for funding the present research.
The authors have declared that no conflicting interests exist.

References

[1] Stern DA, Khanbilvardi R, Alair JC and Richardson W Ecological Engineering 2001 18(**2**): 173. Description of flow through a natural wetland using dye tracer tests.

[2] Viriot M L and Andre JC, *Analysis* 1989 17: 97 Fluorescent dyes: a search for new tracers for hydrology.

[3] Magal E, Weisbrod N, Yakirevich A and Yechieli Y 2008 *Journal of Hydrology* 358 124– 133.

[4] Benedini M and Tsakiris G 2013 Water Quality Modelling for Rivers and Streams Vol 70-ch 17-19. (Dordrecht Heidelberg New York London Springer) Aeby P, Schultze U, Braichotte D, Bundt M, Moser-Boroum F and Hannes Wydler Hannes Flühler 2001 *Environ. Sci. Techno*l 35, **4**, 753-760.

[5] Registry of Toxic Effects of Chemical Substances, Vol I, Cincinnati, Ohio, US Department of Health and Human Services (ed.) (1979)

[6] Smart PL and Laidlaw IMS, 1977 *Water Resources Research* 13 (**1**) 15-33.

[7] Flury M and Wai NN, 2003 *Reviews of Geophysics* 41, **1** / 1002.

[8] Kolb M and Franz H, 1990 Transport of Rhodamine-B Following a Slug Release into the River Elbe above the Port of Hamburg, pag 189, *Coastal and Estuarine Studies*, Editor W. Michaelis, Berlin Heidelberg Springer Verlag.

[9] Nielsen J H, Pedersen C, Kjorboe T, Nikolajsen T, Brydegaard M and. Rodrigo PJ 2019 *Appl. Opt.* 58(**26**) 7022-7027.

[10] Suijlen J and van LeussenIn W Recent developments in large-scale tracing by fluorescent tracers Michaelis W. (eds) Estuarine Water Quality Management. Coastal and Estuarine Studies (Formerly Lecture Notes on Coastal and Estuarine Studies), vol 36. Page 181 Springer, Berlin, Heidelberg.

[11] Auzel F 2004 *Chem. Rev.* 104 139–174.

[12] Nadort A, Zhao J and Goldys EM 2016 *Nanoscale* **8** 13099–13130.

[13] Lingeshwar Reddy K, Balaji R, Kumar A and Krishnan V 2018 *Small*, 14 (**37**) 1801304.

[14] Zhu X, Zhang J. Liu L and Zhang Y 2019 *Adv. Sci.* Recent 6 1901358

[15] Zhang Z, Shikha S, Liu J, Zhang J, Mei Q and Zhang Y. 2019 *Anal. Chem*. 91 **1** 548–568

[16] Mandl G A, Cooper D R, Hirsch T, Seuntjens J and Capobianco JA 2019 *Methods and Applications in Fluorescence* 7 (**2)** 012004

[17] Cates E L,. Chinnapongse S L, Kim J-H, and Kim J-H 2012 *Environ. Sci. Technol* 46, **22**, 12316–1232.

[18] Haase M. and Schäfer H 2011 *Angew. Chemie Int. Ed*. **50** 5808–5829.

[19] Wang, F and Liu, X 2008 *J. Am. Chem. Soc*. 130, 5642– 5643.

[20] Mahata M, Bae H and Lee K 2017 *Molecules*, **22** 2064.

[21] Kumar P, Singh S and Gupta B K 2016 *Nanoscale **8*** 14297–14340.

[22] Zhou J, Leaño Jr. JL, Liu Z, Jin D, Wong K-L, Liu R-Sh, and Bünzli J-C G 2018 *Small* 14 **40** 1801882.

[23] Wu S, Han G, Milliron D J, Aloni S, Altoe V, Talapin D V, Cohen B E and. Schuck P J, 2009 *Proc Natl Acad Sci 106 (**27**)* 10917–10921.

[24] Zhang J, Li B, Zhang L and Jiang H 2012 *Chem. Commun*. **48** 4860- 4862.

[25] Yi G. S., Chow G. M. 2006 *Adv. Func. Mater.* 2006, 16, 2324.

[26] Ye, X, Collins J E, Kang Y, Chen J,. Chen D T N, Yodh A G., and Murray C B 2010 *PNAS* 107 (**52**) 22430-22435.

[27] Rillings K. W. and Roberts J. E. 1974 *Thermochimica Acta*, 10 285-298.

[28] Johnson N J J, Sangeetha N M., Boyer J-C and van Veggel F C J M, 2010 *Nanoscale* **2** 771–777.

[29] Zhou J, Liu Q, Feng W, Sun Y, and Li F 2015 *Chem. Rev.* 115, **1**, 395–465.

[30] Pollnau M, Gamelin D R, Lüthi S R, Güdel H U and Hehlen M P, 2000 *Phys. Rev. B* 61, 3337–3346.

[31] Qian H-S and ZhangY, 2008 *Langmuir*, 24, 12123-12125.

[32] Mourdikoudis S, Pallares R M and. Thanh N T K 2018 *Nanoscale* **10**, 12871–12934.

[33] Dukhno O, Przybilla F, Collot M, Klymchenko A, Pivovarenko

V, Buchner M, Muhr V, Hirsch T and Mély Y 2017 *Nanoscale*, **9**, 11994-12004.

[34] Wilhelm S, Kaiser M, Würth C, Heiland J, Carrillo-CarrionC. , Muhr V, Wolfbeis O S., Parak W J., Resch-Genger U and Hirsch T, 2015 *Nanoscale*, **7**, 1403-1410.

[35] Koczkur K M., Mourdikoudis S, Polavarapu L, and Skrabalak S E 2015 *Dalton Trans*. 44 17883–17905.

[36] Li Z and Zhang Y 2006 *Angew. Chem. Int. Ed*., 45, 7732 – 7735.

[37] Pattanaik, M.; Bhaumik, S. K. *Mater. Lett.* 2000, 44, 352

[38] Oleksandr K A, Korsun M., Gubin I I, Kovalenko S M., and. Kalugin O N 2015 *J. Phys. Chem. C*, 119, 7888−7899.

[39] Karbowiak M, Cichos J.,. Buczko K 2014 *Journal of Rare Earths,* 32 (**3)** 282.

[40] Karbowiak M., Cichos J, and Buczko K 2014 *J. Phys. Chem. B* 118, 226−239.

[41] Arppe R, Hyppänen I, Perälä N, Peltomaa R, Martin Kaiser M, Würth C, Christ S, Resch-Genger U, Schäferling M and Soukka T 2015 *Nanoscale* **7**, 11746.

[42]. Rabouw F T, Prins PT, Villanueva-Delgado P, Castelijns M, Geitenbeek RG and Meijerink A. 2018 *ACS Nano*, 12, 4812−4823.

[43] Kyrychenko A, Korsun O M,. Gubin I I,. Kovalenko S M and Kalugin O N. *J. Phys. Chem. C* 2015, 119, **14**, 7888−7899.

[44] Lakowicz J R, Principles of Fluorescence Spectroscopy 2006 Third edition (Springer, New York, NY USA).

[45] López Arbeloa F, López Arbeloa T, Tapia Estévez M J, and López Arbeloa I, 1991 *J. Phys. Chem*., 95, 2203-2208.

[46] Ghiggino K.P., Brown, J.M., Launikonis,A, Mau, A.W.-H, and W. H. F. Sasse 1988 *Aust. J. Chem*., 41, 9-18.

[47] Xie L, Qin Y, and Chen H-Y. 2012 *Anal. Chem.*, 84, 1969−1974.

[48] Wu T, Boyer J-C, Barker M, Wilson D, and Branda N R 2013 *Chem. Mater*. 25 **12**, 2495–2502.

[49] Burgess L, Jone A R, Hay S and Natrajan L S 2019 *Methods Appl. Fluoresc*. 7 034003.

[50] Muhr, V., Wurth, C., Kraft, M.,Buchnera, M., Antje J. Baeumnera, A. J., Resch-Genger, U. and Hirsch T, 2017 *Anal. Chem.* 89, 9, 4868–4874.

[51] Ding Y, Wu F, Zhang Y, Liu X,. de Jong E M L D, Gregorkiewicz T, Hong X, Liu Y, Aalders M C G, Buma W J and Zhang H 2015 *J. Phys. Chem. Lett.* 6 2518−2523.

[52] Chen R, Ta V D, Xiao F, Zhang Q and Sun H, 2013 *Small* 9, **7**, 1052–1057.

[53] Chen H and Ren J 2012 *Talanta* 99 404–408.

[54] Valeur B. Molecular Fluorescence Principles and Applications 2002 WILEY-VCH Verlag GmbH, 2002.

[55] Xionga H, Min Q, Ma H, Zhao L, Chen W, Qiu J, Yu X, Xu, X. 2019 *Journal of Rare Earths* 37, **4**, 339-344.